Article

The Efficient Recyclable Molybdenum- and Tungsten-Promoted Mesoporous ZrO$_2$ Catalysts for Aminolysis of Epoxides

Xolani Sibusiso Hlatshwayo, Morena S. Xaba, Matumuene Joe Ndolomingo, Ndzondelelo Bingwa * and Reinout Meijboom *

Center for Synthesis and Catalysis, Department of Chemical Sciences, University of Johannesburg, P.O. Box 524, Auckland Park, Johannesburg 2006, South Africa; mrsbuda.mhayise@outlook.com (X.S.H.); xabams@gmail.com (M.S.X.); joe_ndol@yahoo.fr (M.J.N.)
* Correspondence: nbingwa@uj.ac.za (N.B.); rmeijboom@uj.ac.za (R.M.); Tel.: +27-(0)11-559-2367 (R.M.); Fax: +27-(0)11-559-2819 (R.M.)

Abstract: In the present study, we report the synthesis and catalytic activity of tungsten- and molybdenum-promoted mesoporous metal oxides in the aminolysis of epoxides. The as-synthesized catalysts were fully characterized by a variety of techniques such as transmission electron microscopy (TEM), scanning electron microscopy (SEM), temperature-programmed reduction (TPR) and desorption (TPD), nitrogen sorption measurements, powder X-ray diffraction (p-XRD), and thermogravimetric analysis (TGA). Amongst the two supports utilized, ZrO$_2$ is a better support compared to SiO$_2$. Furthermore, MoO$_3$ proved to be a better dopant compared to its counterpart. Several parameters such as the variation of solvents, substrates, catalyst amounts, and stirring speed were investigated. It was observed that 450 rpm was the optimum stirring speed, with toluene as the best solvent and styrene oxide as the best substrate. Moreover, the optimum parameters afforded 98% conversion with 95% selectivity towards 2-phenyl-2-(phenylamino) ethanol and 5% towards 1-phenyl-2-(phenylamino) ethanol. Furthermore, 5%MoO$_3$-ZrO$_2$ catalyst demonstrated optimal performance and it exhibited excellent activity as well as great stability after being recycled 6 times.

Keywords: mesoporous zirconium oxide; molybdenum; tungsten; selectivity; heterogeneous catalysis; inverse micelle; aminolysis of epoxides

1. Introduction

An increasing interest in the solid Lewis acids has attracted researchers from both industrial and academical fields. The greatest interest is shown in synthesizing new ordered mesoporous structures possessing pores of apparent sizes and shapes [1]. Most investigations have been conducted in such a way that they focus on the expansion of the pore sizes into the mesopore range, permitting larger molecules to enter the pore system to be refined and exit at a later stage [2]. The first synthesis of an ordered mesoporous material was reported around 1968, but due to the lack of sophisticated analysis techniques, the significant features of these materials were not recognized [1,3]. In the late 1980s, Hino and Arata prepared tungstated zirconia (WO$_3$/ZrO$_2$) catalyst which was contemplated as the next solid acid catalyst [4]. In 1992, similar materials known as crystalline mesoporous materials were reported by scientists in Mobil Oil Corporation who discovered a remarkable feature and initiated a whole new field of research which gained a lot of recognition [5–8]. Scientists have managed to synthesize similar materials utilizing different approaches [9]. Later on, it was reported that ZrO$_2$ has higher thermal stability and due to this, it was found to be excellent catalytic support [10]. This then led researchers to have a significant interest in examining MoO$_x$/ZrO$_2$ and WO$_x$/ZrO$_2$ catalysts, since the pure ZrO$_2$ becomes more active upon interaction with the dopant [11].

Mesoporous metal oxides (MMO) captivate a great deal of interest due to the fact that their surface properties and pore structures can be altered with ease [12]. The struc-

tural engineering process of mesoporous metal oxides has created various mesoporous materials, doped materials with distinct pore-structures and chemical compositions [6–8]. Furthermore, the structural properties of MMO induce different reactive sites on the heterogeneous catalyst surface. For example, the acidic sites of the catalyst can be easily induced by addition of a second metal [13]. This enables the synthesis of catalysts for specific reactions.

Several catalysts such as aluminum triflate [14,15], zeolites [16], metal alkoxides [17], montmorillonite clay [18], and titanosilicate [19] have been reported under mild conditions. However, they possess several drawbacks such as limited applications, poor catalytic efficiency, unsatisfactory selectivity, corrosive problems, separation process, and non-reusability, just to mention few [19–22]. Thus, there is a need to generate a heterogeneous catalyst which will minimize these presented drawbacks.

Epoxides are important molecules in organic synthesis due to their reactivity with a wide range of nucleophiles [14]. They are considered as good starting materials for a range of useful materials. They are ring-opened into β-amino alcohols which can be acquired from reacting an epoxide with an excess of amine [23]. For the most part, alkylamines are harder bases compared to aromatic amines; hence, they compete more efficiently with an epoxide for the catalyst surface. This is entirely in line with the 'hard-soft acid-base' theory, but harder amines will turn out to retard the rate of reaction [15,24]. Selectivity and activity studies can be determined by kinetic investigation which provides mechanistic evidence of the chemical processes. Information about the reaction mechanism can sometimes be dictated by a non-kinetics investigation; however, little can be known about the mechanism until its kinetics have been investigated thoroughly [25]. Herein, we report a mild procedure for the conversion of aniline and epoxides into the corresponding β-amino alcohols in excellent yields, using 5% tungsten- and molybdenum-promoted mesoporous ZrO_2 as catalysts (Scheme 1).
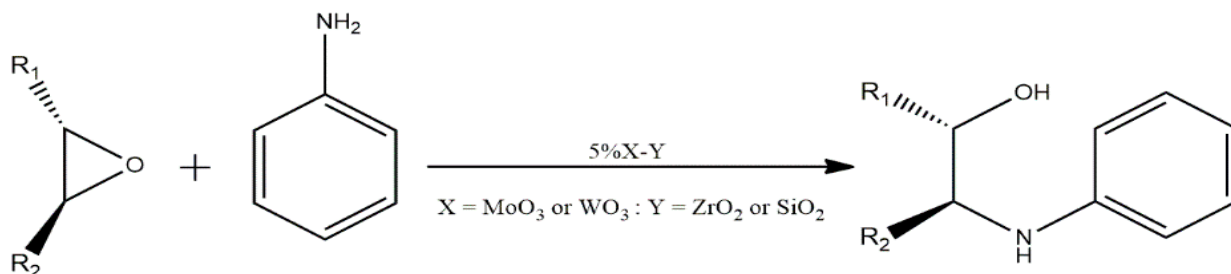
Scheme 1. General formation of β-amino alcohol from an epoxide and aniline.

2. Results and Discussion

2.1. Synthesis and Characterization

Thermally stable mesoporous mixed oxides were synthesized by utilizing a sol–gel synthesis approach [26]. It used HNO_3 to prevent the condensation process and P-123 as the surfactant species. 1-Butanol was used as an interface modifier which compensates for the reduction in aggregation number, prevents the formation of the condensation by generating a physical barrier between oxo-clusters, and also limits the oxidation of the surfactant molecules present in the micelle [27,28]. It was observed that during the mixing process, the tungsten solution turned opaque and viscous, and upon the addition of the molybdenum solution, the gel became dark yellow. These observed color changes were caused by the existence of NO_3^- ions, as stated in the literature [25].

Surface and porosity studies using the nitrogen sorption technique showed the materials as mesoporous in nature with promoted ZrO_2 catalysts revealing pore diameters (P_D) between 11.7 and 12.8 nm. This was also observed for promoted SiO_2 catalysts which were used for comparison. A pore diameter range of 3.7–11.6 nm was obtained. The pore diameter distribution plots can be seen in Figure 1a. The use of molybdenum induced high

surface area (A_{BET}) to the parent zirconia compared to the tungsten counterpart. Surface areas of 44 and 100 m^2/g were obtained when molybdenum was used as a zirconia and silica promoter, respectively, while tungsten as a promoter gave 21.5 and 23 m^2/g for zirconia and silica, respectively. The adsorption–desorption curves of the as-synthesized catalysts also indicate the presence of mesopores. The appearance of hysteresis loops in type IV isotherms is an indication of the mesoporosity of the materials (Figure 1b). Table 1 summarizes the nitrogen sorption, p-XRD, and NH$_3$-TPD results.
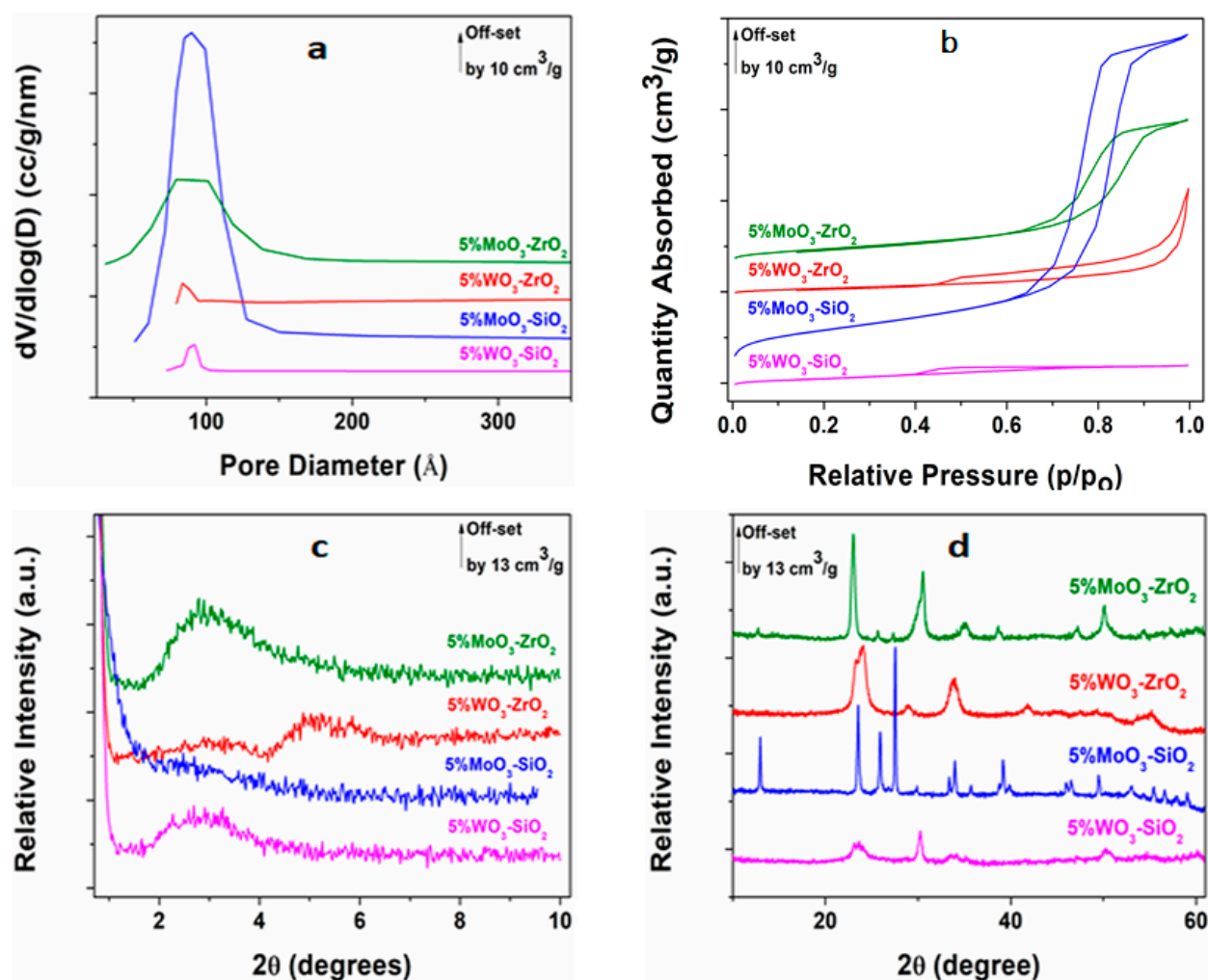

Figure 1. Textural characteristic plots of the as-synthesized MMO; (**a**) BJH desorption pore volume (P_V) distribution, (**b**) N$_2$ sorption isotherms, (**c**) Low-angle p-XRD, and (**d**) Wide-angle p-XRD.

Table 1. Textural characterization and p-XRD data of the as-synthesized catalysts.

Catalyst	A_{BET} (m^2/g)	P_v (cm^3/g)	P_D (nm)	Crystallite Size [a] (nm)	Acidity [b] (mmol/g)
5%WO$_3$-ZrO$_2$	22	0.07	12.8	37.7	2.74
5%WO$_3$-SiO$_2$	23	0.02	3.7	8.1	1.62
5%MoO$_3$-ZrO$_2$	44	0.13	11.7	14.5	0.73
5%MoO$_3$-SiO$_2$	101	0.29	11.6	104.9	0.49

[a] Crystallite sizes calculated from the Scherrer equation using the most intense peak. [b] Surface acid site density = $\frac{total\ acidity}{Surface\ area}$.

The mesoporous nature of these materials was further confirmed by the powder X-ray diffraction results. From the low angle measurements, the appearance of a diffraction peak below 4° 2θ is an indication of mesoporosity (Figure 1c). Interesting results were obtained

from the wide angle, where the crystallinity of the materials was affected by the type of the added promoter. When molybdenum was used as a promoter for both zirconia and silica, the diffraction patterns showed high crystalline materials, while tungsten affected the structure of the two parent oxides and altered them to an amorphous nature (Figure 1d).

The TEM images in Figure S1 display high magnification images which illustrates that the interconnected voids of metal-oxo clusters were distinctly present; these images also illustrate that the crystallites were packed in a regular way, confirming that there were pores present. Furthermore, the dark speckles that are observed on the synthesized 5%WO_3-SiO_2 and 5%WO_2-ZrO_2 MMO can be ascribed to tungsten clusters [4,29]. SEM images in Figure S2 depicted uniform pores all over the materials. Moreover, to confirm the composition of catalysts, energy dispersive X-ray analysis was employed, and it was observed that the as-synthesized catalysts had no impurities (Figure S3).

The thermal stability of the as-synthesized catalysts was studied using thermogravimetric analysis. From thermograms, it is clearly noted that these catalysts are thermally stable below 600 °C (Figure S4). All catalysts depicted dehydration in the temperature range of 30 to 350 °C. A temperature range up to 600 °C, where no weight loss is detected, indicates the thermal stability of the as-synthesized catalysts. There seems to be degradation of the catalyst above the 600 °C mark. It can be seen from the temperature-programmed reduction (Figure S5) that all the synthesized catalysts had two peaks. Furthermore, the occurrence of these multiple reduction peaks indicates the presence of several reducible states of 5%X-Y (X = MoO_3 or WO_3, Y = ZrO_2 or SiO_2). The H_2-TPR profile of pure MoO_3 previously revealed two peaks at 767 °C and 997 °C, respectively [30]. From Figure S5, it was observed that the TPR reduction peaks of 5%MoO_3-SiO_2 and 5%MoO_3-ZrO_2 shifted towards lower temperatures, indicating higher reducibility of the materials compared to pure MoO_3 [31]. In most cases, WO_x samples reduce through three steps as formerly reported [32]. The third peak, therefore, corresponds to the complete reduction of WO_3 to W metal below 1077 °C [33]. The combination of thermogravimetric analysis and temperature-programmed desorption is widely utilized to determine the number of acidic sites as previously reported [34]. Generally, NH_3-TPD is an extensively utilized method for studying the surface acidity of mesoporous metal oxides [35]. The investigation of acidity is driven by their applications as solid acidic catalysts, and to generate materials with higher selectivity and activity, a comprehensive characterization such as temperature-programmed desorption is essential [36]. Thus, the surface acid properties of the as-synthesized catalysts were investigated by NH_3-TPD and summarized in Table 1.

Furthermore, it was reported that looking at NH_3 desorption peaks, the following trends exist: acid sites of weak strength lie around 200 °C, medium strength lies between 200 and 350 °C, and above 400 °C corresponds to strong acid sites [37]. The acquired NH_3-TPD results illustrated that tungsten binds more strongly with the base (NH_3) and this resulted in higher NH_3 desorption temperature, as depicted in Figure S10. Moreover, molybdenum illustrated weak acid strength, as it is noted in Table 1 and Figure S10. However, it was observed that the acidity decreased as the surface area increased. Thus, 5%MoO_3-ZrO_2 showed superior activity, which might be due to correspondence with solvent adsorption on the active sites. Marquez et al. recently reported that this can be related to higher surface area, which is a clear indication of better dispersion of the active phase [38]. However, the doped SiO_2 showed greater surface area as depicted in Table 1 and the obtained activity was lower.

2.2. Optimization of the Catalytic Variables

Various reaction parameters were investigated for deducing optimum reaction conditions. For reaction systems such as the aminolysis of epoxides over heterogeneous catalysts, there are two competing kinetics of the reaction. One of them is the kinetics of the adsorbed activated species and it is desirable for surface catalyzed reactions, while the second type has to do with mass transport into the porous network of the catalyst. The consequence of the mass transport is the fact that it is not possible to determine the actual activity of

the catalyst. Thus, it becomes very important to first study the effect of the mass transport phenomenon. To do this, we first vary the reactive surface area of the catalyst in the reaction to confirm that the reaction is indeed catalytically driven. Variation of the catalyst mass, which is available in the surface area, proved that the reaction is catalytically driven since the rate of the reaction increased with an increase in mass of the catalyst (Figure 2a, Figure S9). The linearity of the slope of the as-synthesized catalyst in Figure 2b against the observed rate is the first indication that the reaction is not diffusion limited.
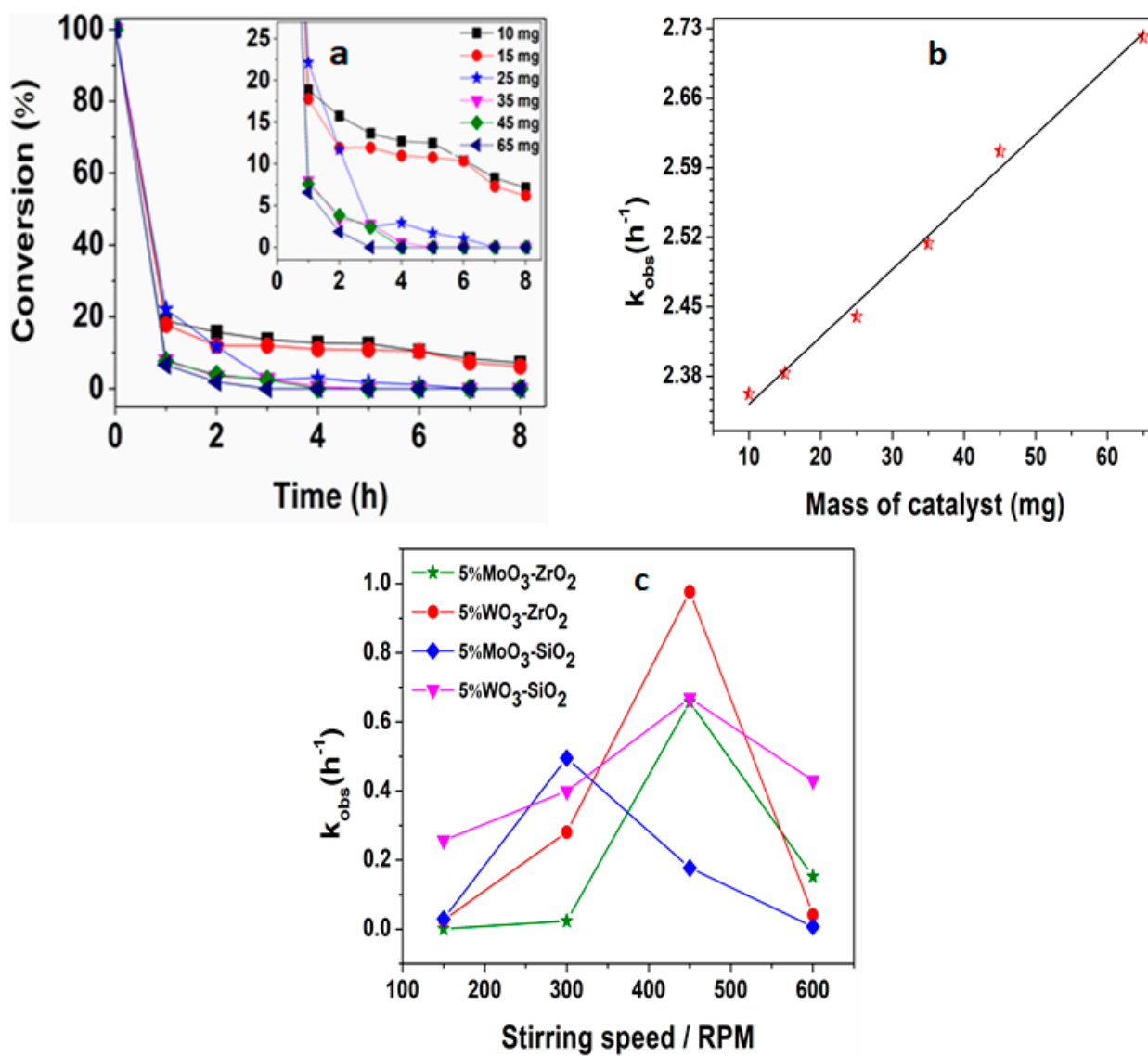

Figure 2. (**a**) Variation of catalyst concentration (5%MoO$_3$-ZrO$_2$), (**b**) initial rate as a function of the catalyst mass (5%MoO$_3$-ZrO$_2$), and (**c**) the influence of stirring speed vs. initial rate on ring opening of cyclohexene oxide utilizing distinct catalysts.

Another way of establishing that the reaction is not diffusion limited is by studying its kinetics by using the reaction stirring rates. Variation of the stirring rates while keeping the reaction parameters the same gives an indication of whether the reaction is dependent on the stirring rate or not. In an event whereby the reaction rate changes with stirring rate, it is an indication of limited mass transport. In this study, we observed that the reaction is only mass transport-limited at low rotations per minute. The reaction rate increases with an increasing stirring rate and reaches an optimum point at 450 rotations per minute. After this point, there is a slight decrease in reaction rates (Figure 2c). This is an indication that

the reaction is independent of mass transport factors and is purely driven by the catalyst. All the other reactions were conducted using 450 rotations per minute.

After establishing that the reactions are not mass transport-limited under the reaction conditions applied, a comparative study of all the synthesized catalysts was undertaken. It is interesting to note that zirconia is known for its activity when applied as an acidic catalyst, while silica has been reported to be inactive, hence the high activities for the zirconia-containing catalysts compared to their silica counterparts (Figure 3a). In both the zirconia- and silica-containing catalysts, molybdenum appears to be the best promoter when compared to silica. From this study, we can conclude that molybdenum is the best promoter and the promoting abilities are not a result of surface area or the amount of acidic sites. The molybdenum-promoted silica has a far greater surface area (100 m^2/g) than the molybdenum-promoted zirconia (44 m^2/g); however, the molybdenum-promoted silica is less active than its zirconia counterpart. The acidic sites of the promoted zirconia catalysts could not be directly correlated to the activity of the catalysts. Tungsten-promoted zirconia has double the acidic sites (0.06) than the molybdenum-promoted zirconia (0.03); however, the activity of the catalysts indicates that molybdenum-promoted zirconia is a better catalyst.
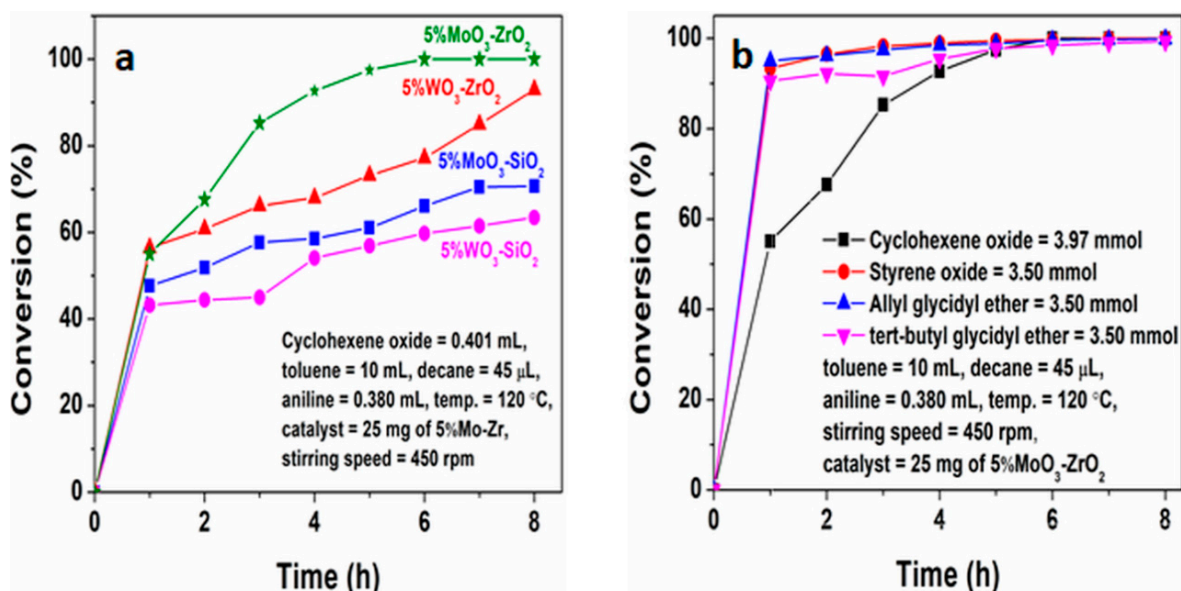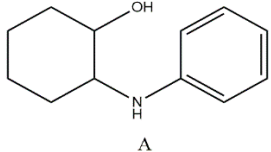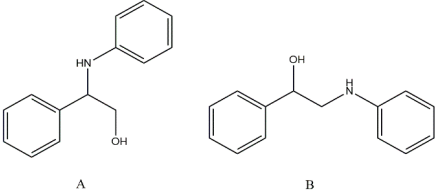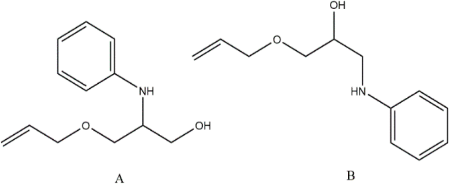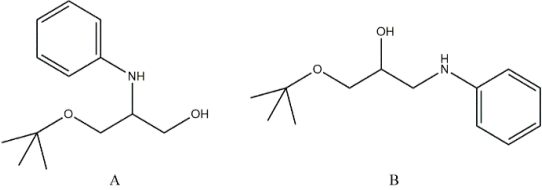

Figure 3. (**a**) The activity of various catalysts on the ring-opening of cyclohexene oxide and (**b**) the ring-opening of several epoxides.

The determination of the best catalyst helped narrow down the number of catalysts. The substrate variation study was performed using the molybdenum-promoted zirconia catalyst, which appeared to be a better catalyst compared to the rest. There were similar reaction rates in most substrates—the aminolysis of styrene oxide, allyl glycidyl ether, tert-butyl glycidyl ether; however, for aminolysis of cyclohexene oxide, there was a slow initial rate observed. All the catalytic reactions using different substrates achieved similar conversion, 100%, after 8 h (Figure 3b).

Apart from substrate variation, the nature of the solvent was also investigated for all the substrates (Table 2 and Figure S6). The preliminary results suggest that there are small deviations in percentage conversions for all solvents when allyl glycidyl ether and cyclohexene oxide are used as substrates (Figure S6a,c) and the gcms technique confirmed the formation of β-amino alcohol as shown in Figure S7 and Figure S8. However, cyclohexane and tetrahydrofuran decreased the activity of the molybdenum-promoted zirconia compared to other solvents such as toluene, hexane and ethanol, as shown in Figure S6b. Moreover, it was observed that in the presence of a donor solvent (THF), product C was

acquired, which is believed to be styrene (Scheme 2). It is worth noting that we were unable to fully identify styrene. Hence, we report it as others (possible product) since Kawaji et al. and RajanBabu et al. pointed out that upon utilizing THF as a solvent in ring-opening of epoxides, the dimer will split to produce the monomeric species regarded as an un-rigid solvated "T-M-C radical (transition metal centered)" [39–41]. In this case, we assume that styrene oxide was deoxygenated to styrene. Furthermore, cyclohexane again proved to be a poor solvent in the ring opening epoxidation of styrene oxide with only conversion of above 10% (Figure S6d).

Table 2. Solvent and substrate variation.

Product(s)	Solvents	Selectivity (%) [a]			Conv. (%)
		A	**B**	**C** [b]	
A	Cyclohexane	100	0		88.6
	Toluene	100	0		85.3
	Hexane	100	0		89.9
	THF	92.6	0	7.45	82.1
	Ethanol	100	0		90.9
A　　　　B	Cyclohexane	94.5	5.47		14.8
	Toluene	95.3	4.73		97.6
	Hexane	92.3	7.75		96.9
	THF	88.6	0	11.4	90.2
	Ethanol	96.7	3.35		94.5
A　　　　B	Cyclohexane	91.5	8.55		97.0
	Toluene	91.6	8.40		97.4
	Hexane	91.8	8.20		75.6
	THF	81.1	6.67	12.3	90.7
	Ethanol	97.9	2.13		95.5
A　　　　B	Cyclohexane	92.6	7.44		58.9
	Toluene	91.8	8.24		91.6
	Hexane	92.0	8.0		96.4
	THF	85.3	5.31	9.38	61.5
	Ethanol	98.9	1.09		85.5

Reaction conditions: 1.2 equiv. aniline, 120 °C. [a] Selectivity towards the major and minor products, time = 3 h. [b] Selectivity towards possible product—styrene. Conv.: Conversion.
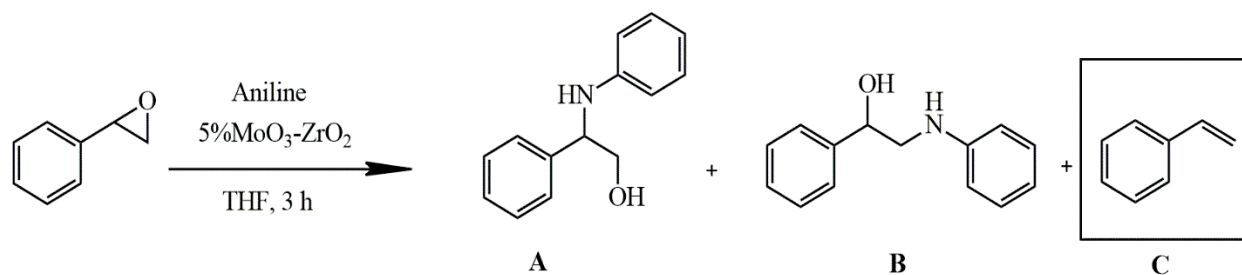
Scheme 2. Reaction of styrene oxide with aniline in the presence of THF, possibly producing styrene resulting from deoxygenation process.

Based on the catalytic results analyzed above, we can conclude that 5%MoO$_3$-ZrO$_2$ afforded higher catalytic activity of the aminolysis of epoxides under optimal parameters. Furthermore, a comparative catalytic study of 5%MoO$_3$-ZrO$_2$ is detailed along with the results published in the literature (Table 3). Our synthesized catalyst afforded higher conversion of 97.4% within 3 h with 25 mg of the as-synthesized catalyst under refluxing system in an inert atmosphere, which confirms that the investigated molybdenum-promoted zirconium is much more effective. However, there is still a need to further optimize our conditions to a point whereby we utilized minimal temperature as well as the solvent-free system. Looking at SBA-15-*pr*-SO$_3$, about the same amount of the catalyst was used under the solvent-free condition; however, the conversion was poor, and the reaction took more time.

Table 3. A direct comparison of effectiveness of 5%MoO$_3$-ZrO$_2$ on the aminolysis of styrene oxide with aniline and those catalyst reported in the literature.

Catalyst	Solvent	Time (min)	Catalyst Amount (mg)	Conversion (%)	Ref.
5%MoO$_3$-ZrO$_2$	Toluene	180	25	97.4	TW
Ti-MCM-41	Toluene	240	50	80.5	[19]
TiO$_2$	nil	240	50	48.0	[19]
SBA-15-*pr*-SO$_3$H	Solvent-free	240	25	38.1	[42]
Zr-Beta	Solvent-free	30	25	40.5	[43]

TW: this work.

2.3. Catalyst Recyclability

The catalyst recycling and reusability study on aminolysis of styrene oxide with toluene as a solvent was investigated by performing six cycling tests. In Figure 4a, it was clearly observed that the catalyst was successfully reused with a minor loss in activity due to a loss of catalyst amount during recycling. Thus, the conversion of 2-phenyl-2-(phenylamino) ethanol showed little deviation in catalyst activity. The selectivity remained unchanged as no minor product was generated within 30 min of the reaction. To confirm the stability of the optimum catalyst after the 6th catalytic run, TEM image was obtained and compared with that of the fresh catalyst and it showed that the mesostructure of the catalyst remained unchanged, which indicated that the catalyst was stable (Figure 4b).
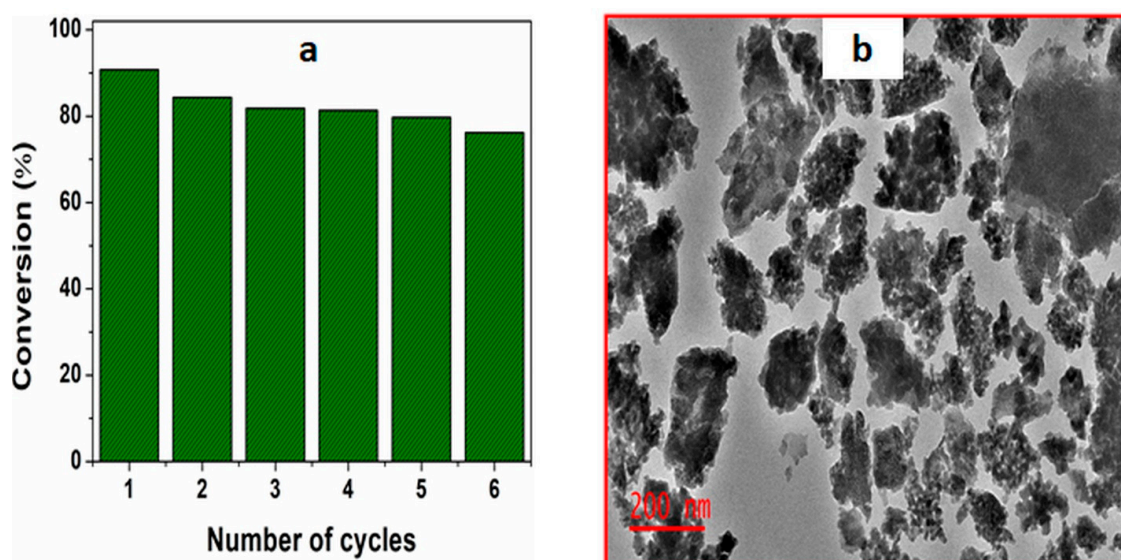

Figure 4. (**a**) The catalytic reusability study: Reaction conditions: 60 mg of 5%MoO$_3$-ZrO$_2$, 10 mL solvent (toluene), temperature = 120 °C, decane = 0.237 mmol, aniline = 4.20 mmol and styrene oxide = 3.50 mmol. (**b**) TEM image taken after the 6th catalytic cycle to confirm the stability of the optimum catalyst.

2.4. Proposed Mechanism

The possible mechanism for this reaction is provided in Scheme 3. A plausible explanation is that 5%MoO$_3$-ZrO$_2$ initially activates an epoxide which induced polarization and made it an easy target for nucleophilic attack by the aniline. Subsequently, there is a possibility that aniline will attack the stable carbon (electron deficient carbon) to form a major product via path 2 or attack less stable carbon from an epoxide (styrene oxide) followed by the protonation process, which ultimately leads to β-amino alcohol.
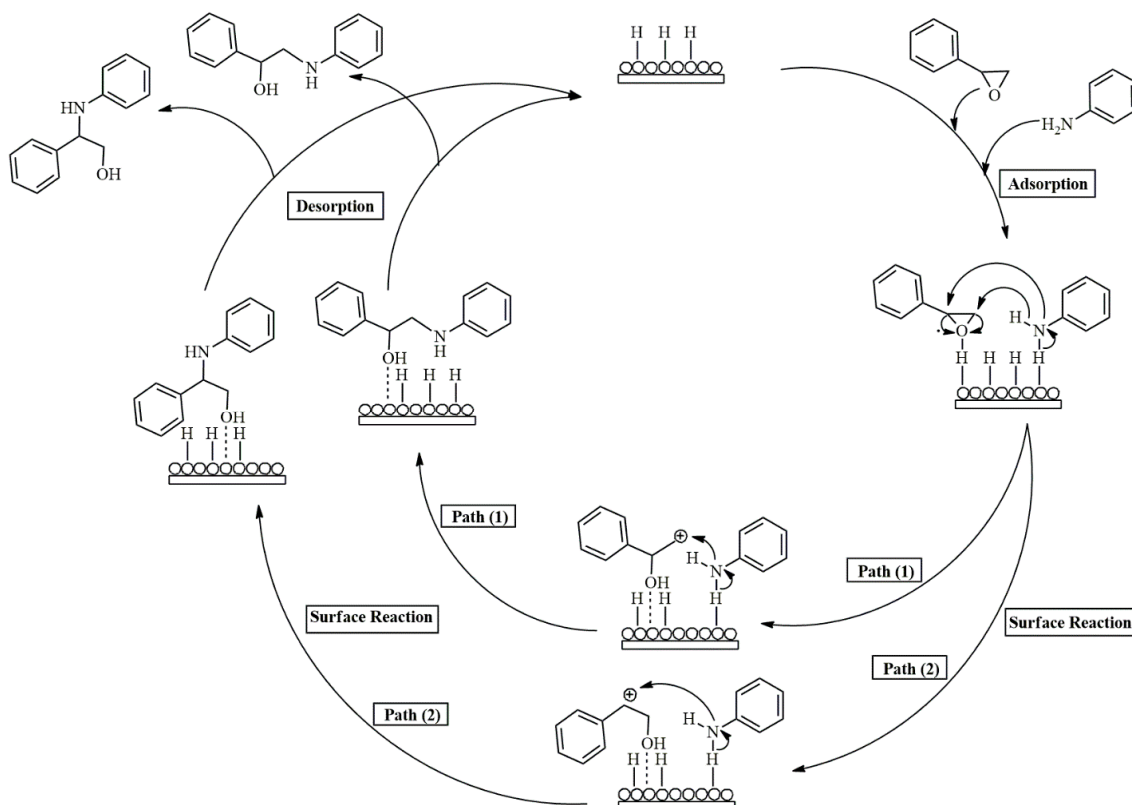
Scheme 3. A plausible pathways for the aminolysis of styrene oxide with aniline in the presence of 5%MoO$_3$-ZrO$_2$.

3. Experiments

3.1. Materials

Ammonium molybdate tetrahydrate (H$_{24}$Mo$_7$N$_6$O$_{24}$·4H$_2$O) (81.0–83.0%), decane (C$_{10}$H$_{22}$) (≥99%), zirconium(IV) oxynitrate hydrate (N$_2$O$_7$Zr·xH$_2$O) (99%), ammonium metatungstate hydrate (H$_{26}$N$_6$O$_{40}$W$_{12}$·xH$_2$O) (≥99.0%), aniline (C$_6$H$_7$N) (99%), tetraethyl orthosilicate (C$_8$H$_{20}$O$_4$Si) (≥99.0%), tert-butyl glycidyl ether (C$_7$H$_{14}$O$_2$) (99%), allyl glycidyl ether (C$_8$H$_{10}$O$_2$) (≥99%), cyclohexene oxide (C$_6$H$_{10}$O) (98%), dichloromethane (CH$_2$Cl$_2$) (≥99.8%), nitric acid (HNO$_3$) (70%), and pol(ethylene glycol)-block-poly(propylene glycol)-block-poly(ethylene glycol) (P123) were purchased from Sigma-Aldrich (Johannesburg, RSA). Styrene oxide (C$_8$H$_8$O) (97%) was purchased from Fluka (Johannesburg, RSA)). Ethanol absolute (C$_2$H$_5$OH) (100%) was purchased from VWR Chemicals (Johannesburg, RSA). Toluene (C$_6$H$_5$CH$_3$) (99.8%) and 1-butanol [CH$_3$(CH$_2$)$_2$CH$_2$OH] (99.5%) were purchased from Rochelle Chemicals (Johannesburg, RSA). All materials were used as received.

3.2. Catalyst Synthesis

The catalysts were synthesized following the procedure that was previously reported by Poyraz et al. [26]. A transition metal precursor (0.02 mol) and 430 μmol of P123 were dissolved in a mixture of 0.19 mol of n-butanol and 0.04 mol of HNO$_3$ in a 300 mL beaker,

and it was stirred at room temperature until the formation of a clear gel. In another 300 mL beaker, a mixture of 0.001 mol of ammonium metatungstate hydrate and 0.001 mol of ammonium molybdate tetrahydrate was dissolved in 2.5 g ethanol plus 2.5 g Milli-Q water to form a transparent mixture. The tungsten and molybdenum %mol added was 5%mol (molX/molY × 100, where X = MoO_3 or WO_3 and Y = ZrO_2 or SiO_2). The solution from the second beaker was then transferred to the clear gel under vigorous stirring, and it was stirred for a further 20 min, and then placed in an oven at 120 °C for 6 h. The obtained materials were further calcined at 600 °C for 1 h under air. The formed brittle materials were ground and labelled 5%X-Y.

3.3. Instrumentation

Nitrogen sorption experiments were conducted on a Micromeritics ASAP 2460 surface area and porosity analyzer at −196 °C. Approximately 0.3 g of the powder samples were degassed for 8 h under nitrogen gas at 90 °C and further degassed for 8 h under vacuum at 250 °C prior to the measurements to remove any adsorbed species. The adsorption–desorption measurements were carried out at −196 °C. The analysis was performed with nitrogen relative pressure (P/P_0) between 0 and 1. The pore diameter (P_D) distribution was calculated using the Barrett–Joyner–Halenda (BJH) method. Low and wide-angle powder X-ray Diffraction (p-XRD) analyses were conducted using a Rigaku MiniFlex-600 diffractometer (Wirsam scientific & precision equipment (PTY) LTD, Johannesburg, RSA) with Cu Kα radiation (λ = 1.5406 Å) at room temperature. Low angle measurements (2θ = 0–10°) were performed with a stepping rate of 0.015°/min and wide-angle (2θ = 10–80°) at a step rate 0.1°/min; the crystallite sizes were calculated using the Scherrer equation: $D = \frac{K\lambda}{\beta \cos\theta}$, with *K* = 0.94. Transmission Electron Microscopy (TEM) images of the mesoporous materials were acquired on a JEOL JEM-2100F electron microscope (Jeol Jem, Boston, MA, USA) with an accelerating voltage of 200 kV. The samples were dispersed in 1 mL ethanol and sonicated for 30 min at room temperature and spotted on a carbon coated copper grid for analysis. Morphology analysis, elemental mapping, and imaging were determined using Tescan Vega 3LMH Scanning Electron Microscopy (SEM) (Wirsam scientific & precision equipment (PTY) LTD, Johannesburg, RSA) with the samples carbon-coated using an Agar Turbo Carbon Coater. The thermal behavior of all the catalysts was investigated by utilizing an SDT Q600 thermogravimetric analyzer (TGA) (Microsep, Johannesburg, RSA) under nitrogen flow with a ramp rate of 10 °C/min from 30 to 1000 °C. The acid sites of the as-synthesized catalysts were verified by the temperature-programmed desorption method (TPD) using a Chemisorption Analyzer Micromeritics AutoChem II 2920 (Micromeretics, Johannesburg, RSA). Hydrogen-temperature-programmed reduction was performed on a Micromeretics AutoChem II machine (Micromeretics, Johannesburg, RSA). Approximately 0.04 g of sample was probed with 10% hydrogen in 90% helium. The analysis temperature was ramped from 25 to 1000 °C with temperature ramping rate of 10 °C/min.

The stirring speed of the reactions was monitored by FMH electronics a 500-watt F3050-0310 magnetic stirrer. For quantitative analysis, a Shimadzu GC-2010 (Shimadzu, Johannesburg, RSA) equipped with a flame ionization detector (FID) and a Restek–800–356–1688 capillary column (30 m × 0.25 mm × 0.25 μm) was used, with temperatures of 250 °C and 300 °C for the injection port and FID, respectively. Specifically, the desired products were confirmed by GC-MS equipped with a capillary column and mass selective detector. The percentage conversions of the desired products were monitored by using GC-FID. A NEYA 8 benchtop centrifuge (Shimadzu, Johannesburg, RSA)) was used for separation.

3.4. Catalytic Evaluation

The 5%X-Y (X = MoO_3 or WO_3 and Y = SiO_2 or ZrO_2) catalytic activities were evaluated through the aminolysis of epoxides under an inert atmosphere and refluxing. Thus, to ensure uniform distribution of the temperature throughout the reaction, a silicone oil bath was used. The experiment was performed under the following conditions: 94.10 mmol of toluene, 0.23 mmol of decane, 4.20 mmol of aniline, and 3.50 mmol of the substrate were

stirred in the round bottom flask, which was embedded inside the temperature-controlled silicone oil bath. The stirring speed of 450 rotations per minute (rpm) was used. In relation to the recyclability of the catalyst, at the end of each cycle, the reaction medium was transferred into a falcon tube where it was topped up with 256.89 mmol of ethanol and centrifuged at 4000 rpm for 15 min. The catalyst was washed three times before it was placed inside the vacuum oven, where it could dry before the next cycle.

4. Conclusions

The sol–gel method was successfully employed in synthesizing doped mesoporous metal oxides. During the optimization process, different experimental parameters were intensely investigated to establish optimum conditions. It was deduced that 450 rpm was obtained as the best stirring speed, styrene oxide as the optimum substrate and lastly, toluene as the optimum solvent. Through investigation of the catalytic activities, the following trend of the solid acid catalysts was observed: $5\%WO_3\text{-}SiO_2 < 5\%MoO_3\text{-}SiO_2 < 5\%WO_3\text{-}ZrO_2 < 5\%MoO_3\text{-}ZrO_2$. Thus, the optimum parameters afforded 98% conversion with 95% selectivity towards 2-phenyl-2-(phenylamino) ethanol and 5% towards 1-phenyl-2-(phenylamino) ethanol. Furthermore, a considerable amount of catalytic activity for the optimum catalyst was still observed after the 6th cycle, with minor loss in its activity and higher selectivity. Interestingly, the optimum catalyst retained its stability, as illustrated by the TEM image taken after the 6th cycle.

Supplementary Materials: The following are available online at https://www.mdpi.com/article/10.3390/catal11060673/s1, Figure S1: TEM analyses of the as-synthesized catalysts; Figure S2: SEM images of the as-synthesized catalysts; Figure S3: EDX characterization of the as-synthesized materials; Figure S4: Thermal gravimetric analysis plots of mesoporous metal oxides: (a) $5\%MoO_3\text{-}ZrO_2$, (b) $5\%WO_3\text{-}ZrO_2$, (c) $5\%MoO_3\text{-}SiO_2$, and (d) $5\%WO_3\text{-}SiO_2$; Figure S5: Temperature-programmed reduction of the synthesized materials; Figure S6: The ring opening efficacy of different substrates under various solvents. The reaction conditions: time = 3 h; catalyst amount ($5\%MoO_3\text{-}ZrO_2$) = 25 mg; stirring speed = 450 rpm; Figure S7: GC-MS spectra for the ring opening of ally glycidyl ether into β-amino alcohol after 4 h of reaction time; Figure S8: GC-MS spectra for the ring opening of tert-butyl glycidyl ether into β-amino alcohol after 4 h of reaction time; Figure S9: Catalyst variation of A:$5\%MoO_3\text{-}ZrO_2$ = 10 mg, B: $5\%MoO_3\text{-}ZrO_2$ = 15 mg, C: $5\%MoO_3\text{-}ZrO_2$ = 35 mg, D: $5\%MoO_3\text{-}ZrO_2$ = 45 mg and E: $5\%MoO_3\text{-}ZrO_2$ = 65 mg at different time intervals; Figure S10: NH3-TPD profiles of MMOs. (a) $5\%MoO_3\text{-}ZrO_2$, (b) $5\%WO_3\text{-}ZrO_2$, (c) $5\%MoO_3\text{-}SiO_2$, and (d) $5\%WO_3\text{-}SiO_2$; Equation S1: Conversion equations.

Conflicts of Interest: The authors declare no conflict of interest.

References

1. Taguchi, A.; Schuth, F. Ordered mesoporous materials in catalysis. *Microporous Mesoporous Mater.* **2005**, *77*, 1–45. [CrossRef]
2. Wei, J.; Sun, Z.; Luo, W.; Li, Y.; Elzatahry, A.A.; Al-enizi, A.M.; Deng, Y.; Zhao, D. New insight into the synthesis of large-pore ordered mesoporous materials. *J. Am. Chem. Soc.* **2017**, *139*, 1706–1713. [CrossRef]
3. Benedicte, L.; Anne, G.; Mika, L. Introduction for 20 years of research on ordered mesoporous materials. *Chem. Soc. Rev.* **2013**, *42*, 3661–3662. [CrossRef]

4. Zhou, W.; Soultanidis, N.; Xu, H.; Wong, M.S.; Neurock, M.; Kiely, C.J.; Wachs, I.E. Nature of catalytically active sites in the supported WO3/ZrO2 solid acid system: A current perspective. *ACS Catal.* **2017**, *7*, 2181–2198. [CrossRef]

5. Kapoor, M.P.; Inagaki, S. Highly ordered mesoporous organosilica hybrid materials. *Bull. Chem. Soc. Jpn.* **2006**, *79*, 1463–1475. [CrossRef]

6. Clark, J.H. Solid Acids for Green Chemistry. *Acc. Chem. Res.* **2002**, *35*, 791–797. [CrossRef]

7. Sayari, A. Catalysis by crystalline mesoporous molecular sieves. *Chem. Mater.* **1996**, *8*, 1840–1852. [CrossRef]

8. Kresge, C.T.; Leonowicz, M.E.; Roth, W.J.; Vartuli, J.C.; Beck, J. Ordered mesoporous molecular sieves sythesized by a liquid-crystal templated mechanism. *Nature* **1992**, *359*, 710–712. [CrossRef]

9. Malgras, V.; Ji, Q.; Kamachi, Y.; Mori, T.; Shieh, F.-K.; Wu, K.C.-W.; Ariga, K.; Yusuke, Y. Templated synthesis for nanoarchitectured porous materials. *Bull. Chem. Soc. Jpn.* **2015**, *88*, 1171–1200. [CrossRef]

10. Tanabe, K. Surface and catalytic properties of ZrO2. *Mater. Chem. Phys.* **1985**, *13*, 347–364. [CrossRef]

11. Xu, J.; Zheng, A.; Yang, J.; Su, Y.; Wang, J.; Zeng, D. Acidity of mesoporous MoOx/ZrO$_2$ and WOx/ZrO$_2$ materials: A combined solid-state NMR and theoretical calculation study. *J. Phys. Chem. B* **2006**, *110*, 10662–10671. [CrossRef] [PubMed]

12. Bartl, M.H.; Puls, S.P.; Tang, J.; Lichtenegger, H.C.; Stucky, G.D. Cubic mesoporous frameworks with a mixed semiconductor nanocrystalline wall structure and enhanced sensitivity to visible Light. *Angew. Chem. Int. Ed.* **2004**, *43*, 3037–3040. [CrossRef]

13. Williams, L.A.; Guo, N.; Motta, A.; Delferro, M.; Fragalà, I.L.; Miller, J.T.; Marks, T.J. Surface structural-chemical characterization of a single-site d0 heterogeneous arene hydrogenation catalyst having 100% active sites. *Proc. Natl. Acad. Sci. USA* **2013**, *110*, 413–418. [CrossRef] [PubMed]

14. Williams, D.B.G.; Lawton, M. Aluminium triflate: A remarkable Lewis acid catalyst for the ring opening of epoxides by alcohols. *Org. Biomol. Chem.* **2005**, *3*, 3269–3272. [CrossRef] [PubMed]

15. Pearson, R.G.; Songstad, J. Application of the principle of hard and soft acids and bases to organic chemistry. *J. Am. Chem. Soc.* **1967**, *39*, 1827–1836. [CrossRef]

16. Kureshy, R.I.; Singh, S.; Khan, N.H.; Abdi, S.H.R.; Suresh, E.; Jasra, R.V. Efficient method for ring opening of epoxides with amines by NaY zeolite under solvent-free conditions. *J. Mol. Catal. A Chem.* **2007**, *264*, 162–169. [CrossRef]

17. Sagawa, S.; Abe, H.; Hase, Y.; Inaba, T. Catalytic asymmetric aminolysis of 3,5,8-trioxabicyclo [5.1. 0] octane providing an optically pure 2-amino-1,3,4-butanetriol equivalent. *J. Org. Chem.* **1999**, *64*, 4962–4965. [CrossRef]

18. Chakraborti, A.K.; Kondaskar, A.; Rudrawar, S. Scope and limitations of montmorillonite K 10 catalysed opening of epoxide rings by amines. *Tetrahedron* **2004**, *60*, 9085–9091. [CrossRef]

19. Satyarthi, J.K.; Saikia, L.; Srinivas, D.; Ratnasamy, P. Regio- and stereoselective synthesis of β-amino alcohols over titanosilicate molecular sieves. *Appl. Catal. A Gen.* **2007**, *330*, 145–151. [CrossRef]

20. Stöcker, M. Biofuels and biomass-to-liquid fuels in the biorefinery: Catalytic conversion of lignocellulosic biomass using porous materials. *Angew. Chem. Int. Ed.* **2008**, *47*, 9200–9211. [CrossRef]

21. Falbe, J.; Bahrmann, H. Homogeneous catalysis-industrial applications. *J. Chem. Educ.* **1984**, *61*, 961–967. [CrossRef]

22. Schmidt, M.; Schreiber, S.; Franz, L.; Langhoff, H.; Farhang, A.; Horstmann, M.; Drexler, H.-J.; Heller, D.; Schwarze, M. Hydrogenation of itaconic acid in micellar solutions: Catalyst recycling with cloud point extraction? *Ind. Eng. Chem. Res.* **2018**, *58*, 2445–2453. [CrossRef]

23. Williams, D.B.G.; Cullen, A. Al(OTf)3-mediated epoxide ring-opening reactions: Toward piperazine-derived physiologically active products. *J. Org. Chem.* **2009**, *74*, 9509–9512. [CrossRef]

24. Krishnamurty, S.; Roy, R.K.; Vetrivel, R.; Iwata, S. The local hard-soft acid-base principle: A critical study. *J. Phys. Chem. A* **1997**, *101*, 7253–7257. [CrossRef]

25. Laidler, K.J.; Glasstone, S.; Eyring, H. Application of the theory of absolute reaction rates to heterogeneous processes I. The adsorption and desorption of gases. *J. Chem. Phys.* **1940**, *8*, 659–667. [CrossRef]

26. Poyraz, A.S.; Kuo, C.-H.; Kim, E.; Meng, Y.; Seraji, M.S.; Suib, S.L. Tungsten-promoted mesoporous group 4 (Ti, Zr, and Hf) transition-metal oxides for room-temperature solvent-free acetalization and ketalization reactions. *Chem. Mater.* **2014**, *26*, 2803–2813. [CrossRef]

27. Poyraz, A.S.; Kuo, C.-H.; Biswas, S.; King'ondu, C.K.; Suib, S.L. A general approach to crystalline and monomodal pore size mesoporous materials. *Nat. Commun.* **2013**, *4*, 2952. [CrossRef]

28. Boettcher, S.W.; Fan, J.I.E.; Tsung, C.; Shi, Q.; Stucky, G.D. Harnessing the sol-gel process for the assembly of non-silicate mesostructured oxide materials. *Acc. Chem. Res.* **2007**, *40*, 784–792. [CrossRef]

29. Yamamoto, T.; Teramachi, A.; Orita, A.; Kurimoto, A.; Motoi, T.; Tanaka, T. Generation of strong acid sites on yttrium-doped tetragonal ZrO2-supported tungsten oxides: Effects of dopant amounts on acidity, crystalline phase, kinds of tungsten species, and their dispersion. *J. Phys. Chem. C* **2016**, *120*, 19705–19713. [CrossRef]

30. Luan, X.; Yong, J.; Dai, X.; Zhang, X.; Qiao, H.; Yang, Y.; Zhao, H.; Peng, W.; Huang, X. Tungsten-doped molybdenum sulfide with dominant double-layer structure on mixed MgAl oxide for higher alcohol synthesis in CO hydrogenation. *Ind. Eng. Chem. Res.* **2018**, *57*, 10170–10179. [CrossRef]

31. Shan, W.; Shen, W.; Li, C. Structural characteristics and redox behaviors of Ce1-xCuxOy solid solutions. *Chem. Mater.* **2003**, *15*, 4761–4767. [CrossRef]

32. Vermaire, D.C.; Berge, P.C. Van The preparation of WO3/TiO$_2$ and W03/Al$_2$O$_3$ and characterization reduction. *J. Catal.* **1989**, *116*, 309–317. [CrossRef]

33. Iglesia, E.; Barton, D.G.; Soled, S.L.; Miseo, S.; Baumgartner, J.E.; Gates, W.E.; Fuentes, G.A.; Meitzner, G.D. Selective isomerization of alkanes on supported tungsten oxide acids. In *Studies in Surface Science and Catalysis*; Elsevier: Amsterdam, The Netherlands, 1999; Volume 101, pp. 1–99. [CrossRef]

34. Gorte, R.J. What do we know about the acidity of solid acids? *Catal. Lett.* **1999**, *62*, 1–13. [CrossRef]

35. Corma, A. From microporous to mesoporous molecular sieve materials and their use in catalysis. *Chem. Rev.* **1997**, *97*, 2373–2420. [CrossRef]

36. Auroux, A. *Determination of Acid/Base Properties by Temperature Programmed Desorption (TPD) and Adsorption Calorimetry*; Springer: Dordrecht, The Netherlands, 2009; ISBN 9781402096785.

37. Akinnawo, C.A.; Bingwa, N.; Meijboom, R. Metal-doped mesoporous ZrO2 catalyzed chemoselective synthesis of allylic alcohols from Meerwein–Ponndorf–Verley reduction of α,β-unsaturated aldehydes. *New J. Chem.* **2021**, *45*, 7878–7892. [CrossRef]

38. Marquez, C.; Rivera-Torrente, M.; Paalanen, P.P.; Weckhuysen, B.M.; Cirujano, F.G.; De Vos, D.; De Baerdemaeker, T. Increasing the availability of active sites in Zn-Co double metal cyanides by dispersion onto a SiO2 support. *J. Catal.* **2017**, *354*, 92–99. [CrossRef]

39. Kawaji, T.; Shohji, N.; Miyashita, K.; Okamoto, S. Non-Cp titanium alkoxide-based homolytic ring-opening of epoxides by an intramolecular hydrogen abstraction in b-titanoxy radical intermediates. *Chem. Commun.* **2011**, *47*, 7857–7859. [CrossRef]

40. RajanBabu, T.V.; Nugent, W.A. Selective Generation of Free Radicals from Epoxides Using a Transition-Metal Radical. A Powerful New Tool for Organic Synthesis. *J. Am. Chem. Soc.* **1994**, *116*, 986–997. [CrossRef]

41. RajanBabu, T.V.; Nugent, W.A.; Beattie, M.S. Free Radical Mediated Reduction and Deoxygenation of Epoxides. *J. Am. Chem. Soc.* **1990**, *112*, 6408–6409. [CrossRef]

42. Saikia, L.; Satyarthi, J.K.; Srinivas, D.; Ratnasamy, P. Activation and reactivity of epoxides on solid acid catalysts. *J. Catal.* **2007**, *252*, 148–160. [CrossRef]

43. Tang, B.; Dai, W.; Sun, X.; Wu, G.; Guan, N.; Hunger, M.; Li, L. Mesoporous Zr-Beta zeolites prepared by a post-synthetic strategy as a robust Lewis acid catalyst for the ring-opening aminolysis of epoxides. *Green Chem.* **2015**, *17*, 1744–1755. [CrossRef]